Magnetic field dependence of terahertz emission from an optically excited GaAs *p-i-n* diode

S. R. Andrews,* A. Armitage, P. G. Huggard,† C. J. Shaw,‡ and G. P. Moore§
Department of Physics, University of Bath, Bath BA2 7AY, United Kingdom

R. Grey
Department of Electronic and Electrical Engineering, The University of Sheffield, Mappin Street, Sheffield S1 3JD, United Kingdom

(Received 3 December 2001; revised manuscript received 22 April 2002; published 12 August 2002)

The magnetic field dependence of the coherent tetrahertz radiation emitted by a GaAs *p-i-n* diode excited by femtosecond optical pulses has been investigated in the limits that the cyclotron frequency is greater than and smaller than the scattering rate. The variation in emitted power with magnetic field in different polarizations and geometries is in good agreement with the predictions of a simple, quantitative Drude-Lorentz transport model taking into account the radiative properties of electric dipoles at a dielectric interface and the effects of screening and source size. Absolute power measurements are also in agreement with a simpler model based on discharge of the sample capacitance.

DOI: 10.1103/PhysRevB.66.085307 PACS number(s): 78.47.+p, 71.45.Gm, 73.20.Mf, 42.65.Re

I. INTRODUCTION

Terahertz radiation produced by femtosecond optical excitation of semiconductor surfaces has been intensively studied in the last decade in an effort to use it as a probe of carrier dynamics[1] and to exploit it for applications such as spectroscopy[2] and imaging.[3] A variety of different processes have been proposed in order to account for the emission in different systems and under different excitation conditions. In *p-i-n* diodes, for example, Hertzian dipole radiation associated with photocurrent surges in the intrinsic region tends to dominate at low excitation power density.[4] Ultrafast field screening in semiconductors can also impulsively excite radiative plasmons and phonons.[5,6] Yet another possible contribution arises from the time varying displacement current associated with the creation of real and virtual electron-hole pairs in states with nonzero dipole moment.[7] This effect can be large compared with that associated with the current surge mechanism for small electric fields and excitation near the band gap.[8] At high excitation density, typically above 1 $\mathrm{GW\,cm^{-2}}$ where the dc field is effectively screened out, optical rectification becomes dominant in noncentrosymmetric crystals and radiation then arises from the time varying second-order polarization $P^{(2)}=X^{(2)}|E(\omega)|^2$. On (100) GaAs surfaces the latter is nonzero only for non-normal incidence and is highly anisotropic with respect to rotation of the plane of polarization about the surface normal.[9]

The first study of the influence of weak magnetic fields on the emission of coherent tetrahertz radiation from semiconductors illuminated by femtosecond optical pulses was reported by Zhang *et al.*[10] They studied GaAs *p-i-n* diodes illuminated at normal incidence and subject to magnetic fields in the plane of the sample at room temperature. It was found that the tetrahertz emission power in the forward direction varied quadratically with magnetic field up to ~0.2 T reflecting a linear relationship between electron acceleration and magnetic field. This was followed by the work of Some and Nurmikko[11,12] who studied photoexcited electron cyclotron emission with a dephasing time of several picoseconds from GaAs epilayers and doped heterostructures at low temperature in tilted Faraday and Voigt geometries. In the tilted Faraday geometry the component of electron kinetic energy along the magnetic field can reach the threshold for LO phonon emission within a few hundred femtoseconds and intervalley transfer in ~a picosecond for typical field strengths $\sim 10^6\ \mathrm{V\,m^{-1}}$. Thus, the authors inferred the existence of a second-order nonlinear contribution to the cyclotron emission, possibly associated with difference frequency mixing between adjacent Landau levels.[12]

Recently, interest has been aroused by reports of high average power tetrahertz emission from *n*-type InAs surfaces excited by femtosecond near infrared radiation under magnetic fields of several Tesla[13] but the emission mechanism is not yet fully understood.[14] Surface states pin the Fermi level above the conduction-band edge, which leads to the existence of a surface accumulation region in *n* type and an inversion layer in *p*-type material some tens of nanometers in extent and the possibility of plasma oscillations involving both surface and bulk carriers. In addition the excitation energies used so far have greatly exceeded the band gap. Consequently, a highly nonequilibrium carrier population is created within a few tens of nanometers of the surface and effects such as hot electron diffusion and intervalley transfer might play an important role. For these reasons we have studied the variation of tetrahertz emission power with magnetic field for a GaAs *p-i-n* diode. This system is simpler in that it has low (background) doping in the active region, is more homogeneous and can be excited closer to the band edge with available femtosecond laser sources. This has allowed us to compare our results with an elementary quantitative model and thus establish some of the important effects responsible for controlling the emission power in a magnetic field.

II. EXPERIMENT

The sample consisted of a GaAs *p-i-n* structure with layers grown by molecular-beam epitaxy in the following order on a semi-insulating (100) GaAs substrate: 500 nm undoped GaAs, 200 nm n-$5\times10^{17}\,\mathrm{cm^{-3}}$ GaAs, 500 nm undoped

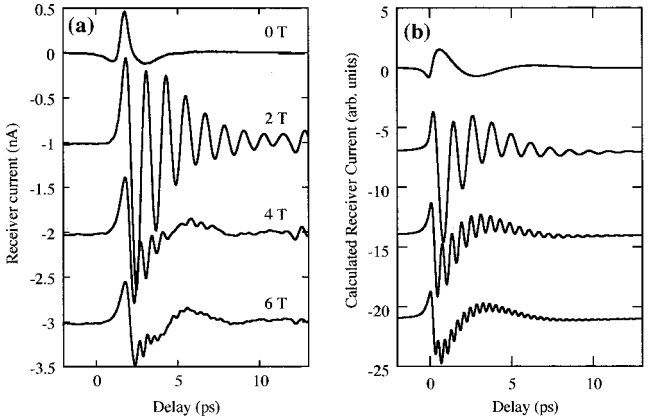

FIG. 1. (a) Experimental *p*-polarized tetrahertz receiver traces for different magnetic fields applied at 45° to the sample surface and in the plane of incidence (excitation energy 1.55 eV, temperature 5 K, pump fluence 30 nJ cm^{-2}). (b) Calculated receiver traces at the same magnetic fields.

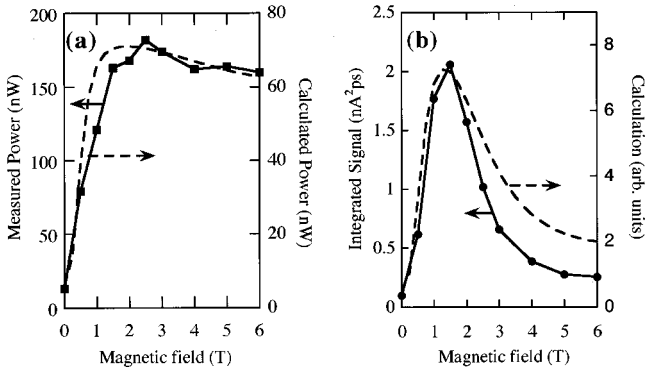

FIG. 2. (a) Experimental (Golay cell) and theoretical variation of emission power with magnetic field for same conditions as Fig. 1 except for larger fluence of 60 nJ cm^{-2}. (b) Experimental and theoretical variation of integrated square of receiver current with magnetic field. Data was obtained under same conditions as that in Fig. 1.

GaAs, and 200 nm p-5×10^{17} cm^{-3} GaAs. Tetrahertz emission was excited with *p* polarized (i.e., electric vector in plane containing excitation and detection axes), 80-fs pulses from a mode locked Ti:sapphire laser at 82 MHz repetition rate. Samples were mounted in a split coil superconducting magnet containing mirrors in the bore such that magnetic fields could be applied at 45° (tilted Faraday geometry) or 90° (Voigt geometry) to the sample surface and in the plane of optical incidence while maintaining a pump angle of incidence of 45°. Measurements were made without electrical bias. We note that attempts to control the field using an external bias were not successful under illumination. Time resolved coherent detection of the tetrahertz electric field radiated in the specular reflection direction was achieved using an optically gated photoconductive antenna. The 10-μm-long dipole antenna was fabricated on an ion implanted silicon/oxide/silicon substrate and had a noise equivalent power of $\sim$100 aW/$\sqrt{}$Hz and a useful bandwidth in excess of 3 THz. Time-integrated detection was performed using a diamond window Golay cell which has an essentially frequency independent responsivity above 0.1 THz. The Golay cell was calibrated using three independent methods and is believed to be accurate to $\pm$20%. Optical coupling of the tetrahertz emission to the receiver was achieved using off-axis parabolic mirrors and a hyperhemispherical silicon substrate lens in the standard configuration. The polarization of the tetrahertz beam was defined using a free-standing wire grid. The photoconductive receivers, which are intrinsically polarization sensitive, can be rotated about the optical axis to detect both *p*- and *s*-polarized emission from the sample. Optical paths were purged with dry air so as to minimize absorption by water vapor.

Figure 1(a) shows *p*-polarized tetrahertz traces in the tilted Faraday configuration with excitation at 1.55 eV. This data (later referred to as low fluence data) was obtained at 5 K with an average pump power of 0.18 W, 3-mm-diameter pump beam (full width at half maximum), and a fluence of 30 nJ cm^{-2}. Fluence figures refer to powers measured outside the cryostat. The illuminated area was measured with the aid of a beam profiler. The exponentially damped sinusoidal oscillations arise from the impulsive excitation and subsequent dephasing of cyclotron motion. The cyclotron frequency $\omega_c = eB/m$ corresponds to an effective mass $m = 0.067m_c$ and the dephasing time is $\sim$2–3 ps. The receiver current is proportional to the tetrahertz electric field that is in turn proportional to the time derivative of the transient photocurrent in the sample. The qualitative shape of the trace in Fig. 1(a) at zero magnetic field is thus understood as follows. The large positive peak and subsequent smaller negative dip reflect the derivative of the steplike increase and slower decrease in the photocurrent following photoexcitation. The initial negative dip is associated with the frequency dependence of the tetrahertz beam focal diameter relative to the dipole length of the receiver antenna.[15] Under magnetic field there is a reversal of the polarity of the main peak [seen more clearly in Fig. 3(a)] and an increase in amplitude. The polarity reversal reflects the change in the average direction of acceleration in the horizontal plane relative to the dipole antenna and the increase in amplitude the fact that the acceleration tends towards the sample surface with increasing field. This behavior is dependent on the magnetic-field geometry and is reproduced by model calculations such as those shown in Fig. 1(b) which are discussed in Sec. III.

Figure 2(a) shows the variation in detected tetrahertz power with magnetic field measured directly using the Golay cell under the same conditions used in obtaining Fig. 1(a) except for a doubling of the fluence to 60 nJ cm^{-2}. This increase in fluence quadrupled the emission power and made accurate measurements with the Golay cell, which has a noise equivalent power of 3 nW/$\sqrt{}$Hz at a chopping frequency of 8 Hz, more accurate. The *p*-polarized power, corrected for detector collection efficiency and reflection losses from the high-resistivity silicon magnet windows, reaches a weak maximum of 175$\pm$50 nW at 2.5 T. Figure 2(b) shows a measure of the emitted power obtained indirectly by squaring the photoconductive receiver traces [Fig. 1(a)] and integrating with respect to time. The strong peak in integrated signal at $\sim$1.5 T is an artifact of the finite antenna bandwidth. The variations of both the directly and indirectly mea-

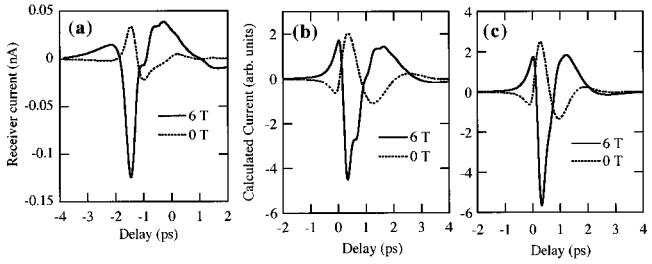

FIG. 3. (a) Experimental *p*-polarized tetrahertz receiver traces for zero magnetic field and for a magnetic field of 6 T applied at 45° to the sample surface (excitation energy is 1.65 eV, temperature 5 K, pump fluence 3.5 μJ cm^{-2}). Calculated receiver traces for (b) $\tau_s = 0.5$ ps, $\eta = 25$ and (c) $\tau_s = 0.3$ ps, $\eta = 5$.

sured emission power with magnetic field are reproduced in model calculations illustrated in Fig. 2 and described in Sec. III where we refer to the above measurements as the low fluence data.

In the data presented above, the cyclotron frequency is large compared with the scattering rate. The opposite limit can be achieved by increasing the temperature, excitation energy, or fluence. For example, increasing the excitation energy to 1.62 eV, while keeping the other parameters fixed, reduces the dephasing time to ~0.8 ps. We attribute this to rapid intraband relaxation by the emission of optic phonons. Figure 3(a) shows receiver current measurements made at 10 K with excitation at 1.62 eV, a pump power of 0.36 W, 400-μm-diameter pump beam, and a pump fluence of 3.5 μJ cm^{-2}. The magnetic field was at 45° to the surface in the same tilted Faraday geometry used in obtaining Figs. 1 and 2. The combination of 2 order of magnitude increase in fluence and larger excitation energy leads to a much reduced scattering time of ~0.3–0.5 ps and the heavily damped cyclotron oscillations are barely discernable in the receiver signal. The extra damping effect at the larger fluence is thought to arise from increased carrier-carrier scattering[16] at the photoexcited electron density of 5×10^{16} cm^{-3}. We did not measure the absolute emission power in the high fluence case and instead studied the emission with the photoconductive receiver (Fig. 4). In the tilted Faraday configuration, Fig. 4(a), the integrated receiver signal increases with magnetic field and passes through a broad maximum in both *p* and *s* polarization. There is no signal at zero magnetic field in *s* polarization because the photocarrier acceleration then has no component along the polarization axis of the detection system. Figure 4(b) shows results for the case of magnetic field parallel to the surface and in the plane of the excitation and detection axes (Voigt geometry). In *p* polarization the integrated signal decreases with magnetic field. This decrease stems from the fact that, with increasing magnetic field, the component of photocarrier acceleration along the polarization axis is reduced at the expense of that along the orthogonal axis. We henceforth refer to the results shown in Figs. 3 and 4 as the high fluence data.

Figure 5(a) shows photoconductive receiver traces obtained at zero magnetic field for varying pump fluence at 1.55 eV. The structure in the signal following the initial transient is associated with radiation from oscillations of the in-

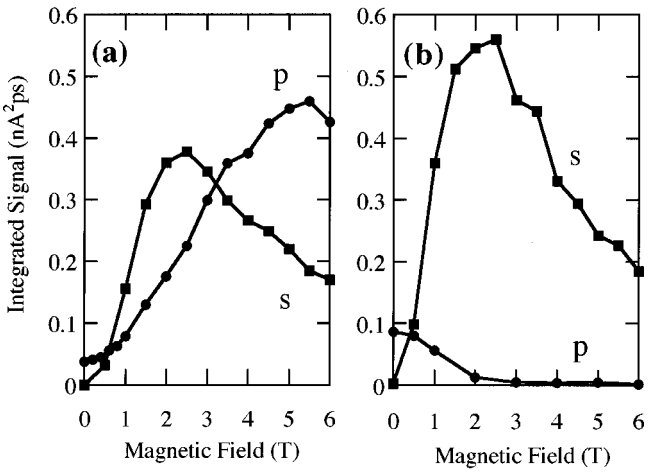

FIG. 4. Experimental variation of integrated square of receiver current with magnetic field in (a) tilted Faraday and (b) Voigt geometries [same conditions as for Fig. 3(a)].

ternal electric field of the diode initiated by the screening effect of the photoexcited carriers. They do not exactly follow an exponentially damped sinusoidal trend because a distribution of plasma frequencies is produced by inhomogeneous excitation. At low fluence, the mean frequency, as determined by Fourier transformation of the transients, increases in proportion to the square root of the fluence [Fig. 5(b)]. The solid curve in Fig. 5(b) shows the predicted variation in oscillation frequency [Eq. (6) in Sec. III] assuming that the photoexcited carrier density is over estimated by 40%. This gives some idea of how well we know the carrier density. In the calculation we take account of reflection losses from cryostat windows and sample and the change in excitation beam profile due to the 45° angle of incidence.

A key parameter affecting the tetrahertz emission power is the electric field in the intrinsic region of the *p-i-n* diode. The magnitude of this field at the start of each laser pulse is much smaller than that expected in the dark because of the screen-

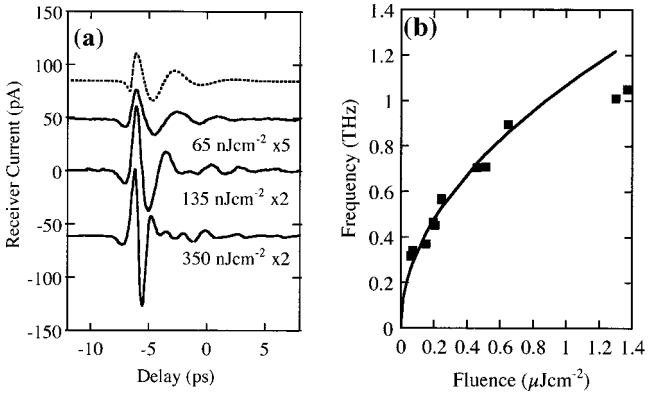

FIG. 5. (a) Photoconductive receiver signals obtained at zero magnetic field for different pump fluence for excitation energy of 1.55 eV and temperature of 10 K. The dotted trace is a calculation for a fluence of 65 nJ cm^{-2} made using the model described in Sec. III. (b) Variation of mean plasmon frequency with pump fluence. The solid curve shows the frequency predicted using Eq. (6) and parameters discussed in the text.

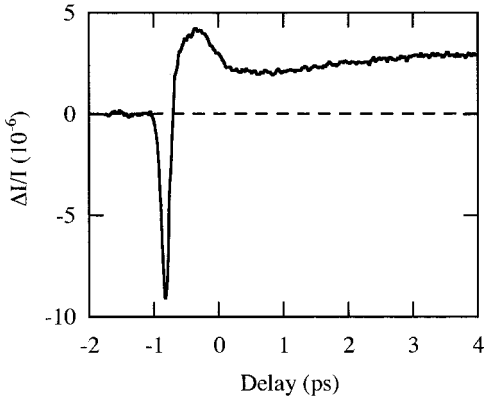

FIG. 6. REOS signal at 1.53 eV for pump fluence of 60 nJ cm^{-2} and temperature of 10 K.

ing action of carriers that accumulate between pulses.[17] We attempted to measure the electric field under the same conditions as used in obtaining the data in Fig. 2(a) by means of reflective electro-optic sampling (REOS). The REOS technique measures a pump-induced rotation of a linearly polarized probe beam[18] reflected from the (100) sample. The incident probe polarization is parallel to the [001] crystal direction. The pump beam was circularly polarized. Both pump and probe were incident within 10° of normal incidence. The rotation of the probe polarization is measured using a polarizing beam splitter and a pair of balanced photodiodes that detect orthogonal polarizations. The difference photodiode current ΔI relative to the single arm current I is related to the change in electric field ΔE parallel to the [001] surface by[17]

$$\frac{\Delta I}{I} = \frac{4n_0^3}{n_0^2 - 1} r_{41} \Delta E. \tag{1}$$

In Eq. (1), n_0 is the refractive index, r_{41} is the clamped electro-optic coefficient, and we have assumed a homogeneous sample. Typical data showing the variation in $\Delta I/I$ with pump-probe delay is shown in Fig. 6. This data was obtained using a 1.55-eV pump beam modulated at 2 MHz, a probe beam modulated at 2.05 MHz and lock-in detection at the difference frequency. The sample was at 10 K and the fluence was 60 nJ cm^{-2}. There are several contributions to the signal; the peaks near zero delay are thought to be associated with interband contributions to the pump-induced optical anisotropy and the slow step change to the intraband polarization producing ΔE. The height of this step increases with decreasing fluence as anticipated. Taking a value[19] for r_{41} of -1.6×10^{-12} V m^{-1} then ΔE from Eq. (1) is 1.3×10^5 V m^{-1}. This is equal to the built-in field, E_b, at the start of the pump pulse because sufficient carriers are injected to completely screen the field after they have transited the intrinsic region in a few picoseconds. For example, at a fluence of 60 nJ cm^{-2} fields up to $\sim3\times10^6$ V m^{-1} (the sheet carrier density divided by the dielectric constant) can be screened. The magnitude of r_{41} above the GaAs band gap is not well known but we believe that our estimate of E_b is likely to be within a factor of 2 of the actual value.

III. MODEL

In this section we present a quantitative model for the tetrahertz emission based on a Drude-Lorentz description of the carrier motion and neglecting nonlinear optical effects. We do not expect that much more involved models based on self-consistent solutions of the Boltzmann transport and Poisson equations or on Monte Carlo simulations would yield results qualitatively very different to those described here. We assume that, because of their smaller mass and greater mobility, the emission principally arises from the acceleration of electrons optically excited in the intrinsic region of the diode and treat the holes as being stationary. Electrons created over the interval of the laser pulse at rate $g(t)$ over the absorption depth are allowed to accelerate under the action of spatially uniform magnetic (B) and electric (E) fields and their position is calculated iteratively as a function of time. The assumption of a spatially uniform electric field appears to be a reasonable one because an electron traverses only a fraction of the intrinsic region over the duration of a typical tetrahertz transient. A single time τ_s is used to describe the effect of all scattering processes and is assumed to be independent of magnetic field. Photocarriers with number density N, effective mass m, and velocity $\boldsymbol{v}$ are allowed to contribute to the photocurrent density $\boldsymbol{j}=Nq\boldsymbol{v}$ for a ''capture'' time τ_c before they enter a region of lower electric field. The equations governing the photocurrent are then

$$\frac{d\boldsymbol{v}}{dt} = -\frac{\boldsymbol{v}}{\tau_s} + \frac{q}{m}[\boldsymbol{E}(t) + \boldsymbol{v}\times\boldsymbol{B}], \tag{2}$$

$$\frac{dN}{dt} = -\frac{N}{\tau_c} + g(t). \tag{3}$$

Time-dependent screening of the electric field by the spatial separation of electrons and holes is taken into account by introducing a local field $\boldsymbol{E}(t)$ and space charge polarization $P_{\rm sc}$:

$$E_x(t) = E_b - \frac{P_{\rm sc}}{\varepsilon_\infty \eta}, \tag{4}$$

$$\frac{dP_{\rm sc}}{dt} = -\frac{P_{\rm sc}}{\tau_r} + j_x, \tag{5}$$

where E_b is the built-in field along the surface normal (x axis) and ε_∞ is the high-frequency dielectric constant. Although we include the recombination time τ_r in Eq. (5) we assume that it is much longer than τ_s or τ_c so that the first term on the right-hand side of Eq. (5) can be neglected. A phenomenological screening parameter η has been introduced in Eq. (4) in the manner described by Jepsen, Jacobsen, and Keiding.[15] The optical absorption depth is small compared with the diameter of the illuminated area so that a slab of charge is photoexcited and η should be unity. The polarization term in Eq. (4) provides a restoring force and for zero magnetic field leads to an oscillatory component of the photocurrent with angular frequency

$$\omega_j \approx \sqrt{\mathrm{Ne}^2/(\eta\varepsilon_\infty m) - 1/(4\tau_s^2)}. \tag{6}$$

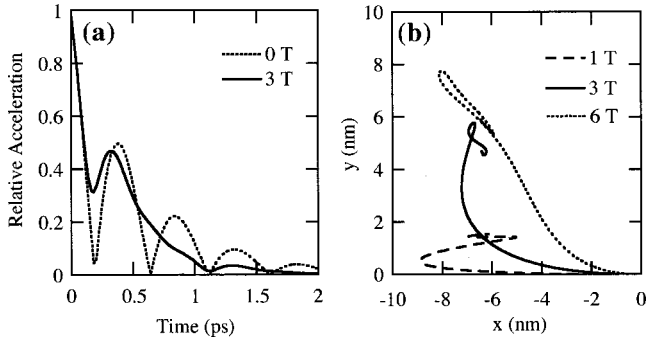

FIG. 7. (a) Calculated time dependence of magnitude of electron acceleration at 0 and 3 T in units of eE_b/m. (b) Electron trajectories for 2 ps following photoexcitation at different magnetic fields. Model parameters are $\tau_s=0.3$ ps, $\tau_c=5$ ps, $\eta=5$, $E_b=1.3\times10^5$ V cm^{-1}, and fluence 3.5 μJ cm^{-2}. The magnetic field is parallel to $[-110]$.

Equation (6) is in agreement with the data shown in Fig. 5(b) for $\eta=1$ assuming an experimental error in the fluence of $\sim$50%. In the absence of scattering ω_j can then be identified with the electron plasma frequency. However, for the highest fluence data [Figs. 3(a) and 4] the best agreement is obtained using values of η of 5 or more. To a first approximation the effect of increasing η in Eq. (4) is similar to reducing the fluence but we believe that a factor of 5 reduction is too large for this to be the only explanation. Physically, a higher value of η corresponds to a weaker than expected depolarizing field although we do not have an explanation for why this should occur. We assume that the larger value is required due to a combination of errors in the measurement of fluence and simplifications inherent in our model. However, we should point out that the precise choice of η does not greatly affect the variation of tetrahertz emission power with magnetic field, which is the main subject of this study.

Neglecting scattering, Eq. (2) predicts an acceleration parallel to $\boldsymbol{B}$ of $(qE/m)\cos\beta$ where β is the angle between $\boldsymbol{B}$ and $\boldsymbol{E}$. The components of acceleration perpendicular to $\boldsymbol{B}$ are $(qE/m)\sin\beta\cos\omega_c\tau$ in the plane of $\boldsymbol{E}$ and $\boldsymbol{B}$ and $(qE/m)\sin\beta\sin\omega_c t$ perpendicular to that plane. Thus, it is apparent that the magnitude of the acceleration is not increased by application of the magnetic field and that the main effect is simply a change in the direction of acceleration. Examples of calculations for $\boldsymbol{B}$ parallel to $[-110]$ that support this picture are shown in Fig. 7. Figure 7(a) shows the magnitude of the acceleration relative to eE_b/m as a function of time at 0 and 3 T. Figure 7(b) shows electron trajectories for 2 ps after photoexcitation and demonstrates steering of the motion toward the surface with increasing field. The sample axes are defined in Fig. 8(a). The parameters used in the calculation are $\tau_s=0.3$ ps, $\tau_c=5$ ps, $\eta=5$, and $E_b=1.3\times10^5$ V m^{-1}. These values qualitatively describe the magnetic field dependence of the high fluence data quite well as discussed in detail in Sec. IV.

Once $\boldsymbol{j}(t)$ is known then the radiated electric fields and the time-average radiation power in the far field can be calculated. In the point-dipole approximation, the power emitted into unit solid angle in the horizontal plane containing the incident and reflected light is (using the notation of Lukosz[20]):

$$I_{p,s}(\alpha_2)\approx\frac{nV^2}{6\pi\varepsilon_o c^3 T}\int_0^T\left(\frac{\partial j}{\partial t}\right)^2 P_{p,s}[\theta(t),\phi(t),\alpha_2]dt. \tag{7}$$

In Eq. (7) and Fig. 8(a), α_2 is the external emission angle measured relative to the surface normal which defines the x axis. T is the laser repetition period and θ is the angle between $\boldsymbol{j}$ and the x axis. The angle $\boldsymbol{j}$ makes with the plane containing the y, excitation and detection axes is described by the corresponding azimuthal angle ϕ. P_p and P_s are factors for p- and s-polarized emission, respectively, which take account of the optical transmission coefficient and change in solid angle on passing from semiconductor to vacuum. In the point-dipole approximation the current is assumed to be confined in a volume V small in each dimension compared with the emission wavelength in the semiconductor (λ_s). In the limit that the excited region lies within a small fraction of λ_s of the surface then[20]

$$P_p=\frac{3}{2\pi}\frac{\cos^2\alpha_2(\cos\theta\sin\alpha_1+\sin\theta\cos\phi\cos\alpha_1)^2}{n(\cos\alpha_1+n\cos\alpha_2)^2}, \tag{8}$$

$$P_s=\frac{3}{2\pi}\frac{\cos^2\alpha_2\sin^2\theta\sin^2\phi}{n(n\cos\alpha_1+\cos\alpha_2)^2}. \tag{9}$$

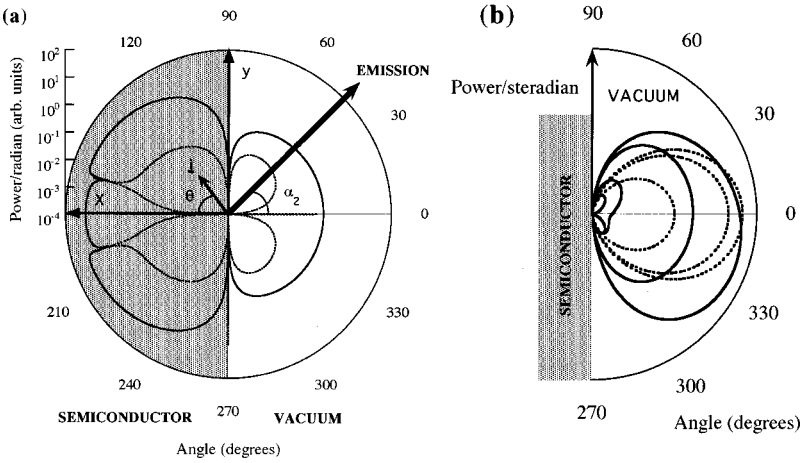

FIG. 8. (a) Angular distribution (log scale) of radiated power for point dipoles perpendicular ($\theta=0$, $\phi=0$ inner curve) and parallel ($\theta=\pi/2$, $\phi=0$ outer curve) to a GaAs surface. (b) Time integrated p-polarized (continuous) and s-polarized (dashed) radiation patterns (linear scale) in the emission plane for a point source calculated using the same parameters as for Fig. 7. The patterns are, in order of increasing power, for magnetic fields of 0, 2, 4, and 6 T. (There is no emission in s polarization at 0 T).

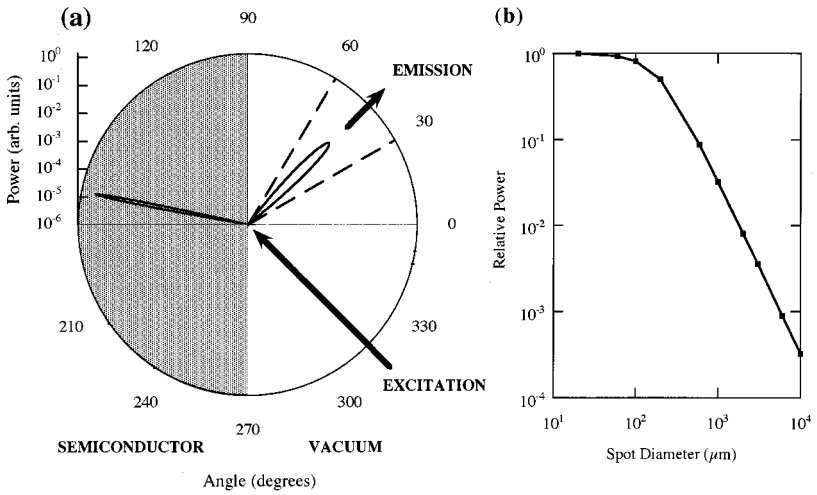

FIG. 9. (a) Angular distribution of radiation for dipoles at 45° to surface when excited with a 45° incident, 3-mm-diameter Gaussian pump beam. Power scale is the same as for Fig. 8(a). (b) Emission power at 1 THz (into cone of acceptance of detection system indicated by dashed lines) of extended dipole source at 45° to surface relative to point source as a function of source diameter.

In Eq. (8) and (9) the internal emission angle α_1 is related to α_2 by $\sin\alpha_1 = \sin\alpha_2/n$, where the tetrahertz refractive index $n=3.62$ for undoped GaAs. The assumption of a frequency independent refractive index equal to that of the substrate in our layered sample is reasonable when considering the long wavelength and small absorption in the thin doped regions.

The radiated tetrahertz electric fields, which are proportional to $|d_j/dt|P_{p,s}{}^{1/2}$, can also be evaluated for comparison with photoconductive receiver data (see Sec. IV). In the far field they are given by

$$E_p(t) = \frac{V}{4\pi\varepsilon_0 c^2 r}\,\frac{\cos\alpha_2}{(\cos\alpha_1 + n\cos\alpha_2)} \times\left(\sin\alpha_1\frac{\partial j_x}{\partial t} + \cos\alpha_1\frac{\partial j_y}{\partial t}\right), \tag{10}$$

$$E_s(t) = \frac{V}{4\pi\varepsilon_0 c^2 r}\,\frac{\cos\alpha_2}{(n\cos\alpha_1 + \cos\alpha_2)}\,\frac{\partial j_z}{\partial t}. \tag{11}$$

The angular terms in Eqs. (8) and (9) are responsible for an increase in radiated power with magnetic field in those geometries in which the component of acceleration along the polarization axis of the detection system is increased. In the absence of a dielectric interface this is a small effect. In the presence of the dielectric interface, however, total internal reflection suppresses emission into vacuum by a perpendicular dipole when compared with a parallel one. This leads to the well-known effect that a dipole parallel to a dielectric interface has a higher radiative efficiency into the low index medium than one perpendicular.[20,21] This is illustrated in Fig. 8(a) which shows the radiation patterns for point dipoles at a GaAs-vacuum interface. These patterns are obtained by integrating Eqs. 8 and 9 over ϕ. The ratio of the total *p*-polarized power emitted into vacuum for a point dipole parallel to the interface compared with one perpendicular is ~12 for GaAs. If we consider specifically the tilted Faraday geometry in *p*-polarization then the effect of increasing the refractive index is to reduce the emitted power at all magnetic fields but in such a way as to increase the ratio of power at large field to that at small field. In the limit $n \gg 1$, the power varies as n^{-4} for small B and n^{-2} for large B. This leads to an enhancement of emission power by a factor of order n^2 at high magnetic field. Figure 8(b) shows the time-averaged radiation patterns corresponding to the electron trajectories in Fig. 7(b) and calculated using Eq. (7). The change in pattern from that characterizing a dipole perpendicular to the semiconductor surface to that of one more parallel, together with the increase in radiated power as the magnetic field is increased, can be clearly seen.

To calculate the radiated power quantitatively, account must be taken of the finite source size by performing a Fraunhofer summation of Eq. (7) over the excitation volume[22] and integrating over the solid angle accepted by the detector. The excitation volume is taken as the width of the intrinsic region d multiplied by the illuminated area A. Interference leads to a narrowing of the angular distribution that becomes centered about the specular reflection direction and a net reduction in radiated power[21] as shown for dipoles oriented at 45° to the surface in Fig. 9(a). The reduction in power becomes larger with increasing illuminated area as shown in Fig. 9(b). If the diameter of the illuminated area is small compared with the emission wavelength then superradiant behavior with emission power proportional to the square of the number of dipoles is expected [this is implicit in Eq. (7)]. In the opposite limit the phase variation between different dipoles leads to a linear dependence of power on the number of dipoles. For a Gaussian pump beam having a 3 mm diameter (full width at half maximum) and for dipoles at 45° to the surface the total power emitted into vacuum at 1 THz is reduced by a factor of ~570 compared with a point source. In making this estimate we have assumed that the dephasing time is longer than or comparable with the time taken for light to traverse the illuminated area so that the relative phase of the dipoles is determined only by their position with respect to the excitation wave front. This is clearly an approximation. For example, if we consider the low fluence data then light takes ~10 ps to traverse the illuminated area, which is longer than the dephasing time of ~2.5 ps. In consequence, our power estimates will tend to be underestimates.

IV. DISCUSSION

Examples of calculated *p*-polarized receiver current traces obtained by convolution of Eq. (10) with the receiver ampli-

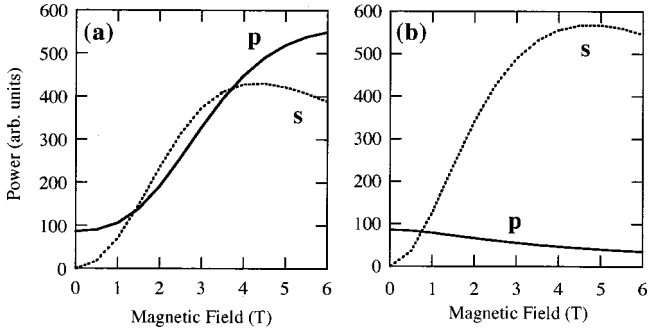

FIG. 10. Calculated variation in *p*- (solid curve) and *s*-polarized (dotted) tetrahertz emission power with magnetic field in (a) tilted Faraday and (b) Voigt geometry for pump fluence of 3.5 $\mu J\,cm^{-2}$. Calculation uses same parameters as for Fig. 7.

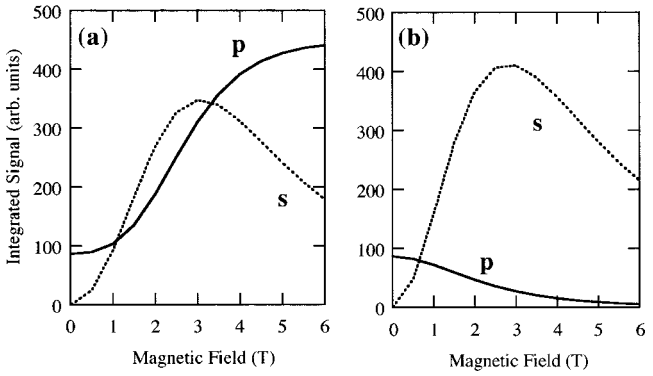

FIG. 11. Calculated variation in integrated receiver signal for *p*- (solid curve) and *s*-polarized (dotted) tetrahertz emission with magnetic field in (a) tilted Faraday and (b) Voigt geometry. Calculation parameters are same as for Fig. 10 but frequency response of receiver is taken into account.

tude response are shown for the conditions of low and high fluence in Figs. 1(b) and 3(b), 3(c), respectively. The receiver response is modeled using the approach described by Jepsen, Jacobsen, and Keiding.[15] Calculations for the low fluence data are based on the choice of parameters $\tau_s = 5$ ps, $\tau_c = 5$ ps, $\eta = 1$, and $E_b = 1.3 \times 10^5$ V m^{-1}. τ_c was chosen as the approximate transit time of electrons in the intrinsic region assuming a drift velocity of 10^5 ms^{-1}. τ_s was chosen so that the dephasing time of the cyclotron oscillations at 2 T was in approximate agreement with experiment. These parameters reproduce the shape of the receiver signals reasonably well [Fig. 1(b)]. For the high fluence data a scattering time of 0.5 ps and a screening parameter $\eta = 25$, with other parameters of the Drude-Lorentz model unchanged from the low fluence case, approximately reproduces the shape of the receiver signals [Fig. 3(b)]. Although these parameters give a good description of the receiver signals, the magnetic field dependence of the integrated signals was best reproduced using $\tau_s = 0.3$ ps and $\eta = 5$. The corresponding receiver signals are shown in Fig. 3(c). This discrepancy undoubtedly reflects the simplicity of our model.

The results of calculations for the variation of tetrahertz emission power with magnetic field made for comparison with the low and high fluence data in Figs. 2 and 4 are shown in Figs. 2(a) and 10, respectively. These calculations used the parameters $\tau_s = 0.3$ ps and $\eta = 5$. The finite bandwidth of the photoconductive receiver leads to differences between measurements made directly with the Golay cell [Fig. 2(a)] and ones made indirectly by integrating the square of the photoconductive receiver current [Fig. 2(b)]. For example, measurements made with the latter, Fig 2(b) reveal a strong peak as a function of magnetic field. This is not apparent in the power measurements made with the Golay cell in Fig. 2(a) that instead show more of a saturation behavior. The behavior seen with the former approach is, however, well reproduced by calculations in which the receiver signal is calculated by convolving the incident electric field with the receiver response function. A direct comparison can thus be made between the experimental and theoretical magnetic field variation of the integrals of the squared receiver current. This is illustrated for the low fluence data in Fig. 2(b). The experimental and theoretical results for the high fluence case are shown in Figs. 4 and 11, respectively. The trends in the measurements made both with the Golay cell and with the receiver as a function of magnetic field are also seen in these calculations. In particular, the magnetic field dependence of the emission power and its dependence on polarization and the direction of the magnetic field are reproduced quite well in both the limits $\omega_c \tau_s > 1$ and $\omega_c \tau_s < 1$. We note that the agreement between experiment and the simple transport model is equally good in both the tilted Faraday and Voigt geometries. In principle, electrons can acquire excess energy from the electric field in the former but not the latter. If carriers acquire excess energies of more than 36 meV then they can emit optic phonons on time scales[23] of ~300 fs and if they acquire more than 300 meV then they may undergo intervalley transfer on time scales of ~100 fs. However, for the relatively small electric field in our sample a ballistically accelerating electron takes more than 4 ps to acquire 36 meV of excess energy. The current surge mechanism is thus consistent with picosecond dephasing times in the low fluence, tilted Faraday experiments [Fig. 1(a)] and it is not necessary to assume that nonlinear processes[12] make a significant contribution.

The accuracy of the absolute power calculation depends mainly on the parameters τ_s (power varies crudely as $1/\tau_s$) and E_b (power varies as $E_b{}^2$) and the assumption of complete source coherence. The choice of screening parameter η has a relatively small effect. The value for τ_s is constrained by the shape of the tetrahertz transients and we have estimated E_b using REOS although there is some uncertainty as to the appropriate value of the electro-optic coefficient. The treatment of source coherence neglects the finite dephasing time so that the power will be underestimated if the condition $\tau_s > \sqrt{A}/c$ is not met as mentioned in Sec. III. For both the low and high fluence experiments, $\tau_s \sim 0.25\sqrt{A}/c$. Another factor is the fraction of photoexcited carriers that actually contribute to the signal. We have assumed that all carriers photoexcited in the intrinsic region contribute equally but those nearest the *p*-type layer will contribute to a lesser extent. It is important therefore to have some additional support for the quantitative aspects of our model. This can be found in a more elementary picture based on energy conservation

although we make the same assumptions regarding source coherence and the magnitude of the electric field. In this model we assume that the action of the excitation pulse is to completely convert the capacitative energy stored in the illuminated portion of the diode into radiation. The average emitted power I is then

$$I \approx \frac{\varepsilon_s A d E_b^2}{2T} f, \tag{12}$$

where f is the fraction of power emitted in the detector direction compared with the total power radiated by the same source in vacuum and ε_s is the static dielectric constant. For illumination with a 3-mm-diameter Gaussian beam f is $\sim 10^{-4}$ if we make the approximation that the average acceleration is at 45° to the surface which is approximately the case for large magnetic field in the tilted Faraday geometry [see Fig. 7(b)]. Under these conditions $I \sim 60$ nW for $E_b = 1.3 \times 10^5$ V m^{-1}. This power is consistent with the predictions of the Drude-Lorentz model [Fig. 2(a)] that treats the electron trajectories more realistically. The fact that both approaches underestimate the observed emission power by a factor of ~ 3 is consistent with the likely errors associated with the common assumptions.

V. SUMMARY

We have presented experimental data on the effects of magnetic field on the tetrahertz emission from a GaAs *p-i-n* diode excited by a femtosecond laser under different experimental conditions. A model based on solving simple transport equations and which takes account of the radiative properties of dipoles at a surface describes the essential qualitative behavior of the electric-field transients and the radiated power with changing magnetic field, experimental geometry, and carrier scattering rate. Including the effects of source coherence leads to reasonable quantitative agreement between experiment and the transport model in the limit of long dephasing times for which we made absolute power measurements. The results are also in quantitative agreement with a simpler model based on discharge of the sample capacitance.

ACKNOWLEDGMENTS

We thank the UK Engineering and Physical Science Research Council for financial support.

*Corresponding author. Email address: s.r.andrews@bath.ac.uk
†Present address: Space Science and Technology Department, Rutherford Appleton Laboratory, Chilton, OX11 0QX, UK.
‡Present address: BAe Systems, Millbrook, Southampton S09 7QG, UK.
§Present address: Laboratoire des Solides, Associe CNRS, Orsay 91405, France.

[1] M. C. Nuss, P. C. M. Planken, I. Brener, H. G. Roskos, M. S. C. Luo, and S. L. Chuang, Appl. Phys. B: Lasers Opt. **58**, 249 (1994).
[2] D. Grischkowsky, S. Keiding, M. van Exter, and Ch. Fattinger, J. Opt. Soc. Am. B **7**, 2006 (1990).
[3] B. B. Hu and M. C. Nuss, Opt. Lett. **20**, 1716 (1995).
[4] B. B. Hu, A. S. Weling, D. H. Auston, A. V. Kuznetsov, and C. J. Stanton, Phys. Rev. B **49**, 2234 (1994).
[5] W. Sha, A. L. Smirl, and W. F. Tseng, Phys. Rev. Lett. **74**, 4273 (1995).
[6] R. Kersting, J. N. Heyman, G. Strasser, and K. Unterrainer, Phys. Rev. B **58**, 4553 (1998).
[7] T. Dekorsy, H. Auer, C. Waschke, H. J. Bakker, H. G. Roskos, H. Kurz, V. Wagner, and P. Grosse, Phys. Rev. Lett. **74**, 738 (1995).
[8] A. V. Kuznetsov and C. J. Stanton, Phys. Rev. B **48**, 10 828 (1993).
[9] X.-C. Zhang, Y. Jin, K. Yang, and L. J. Schwalter, Phys. Rev. Lett. **69**, 2303 (1992).
[10] X.-C. Zhang, Y. Jin, T. D. Hewitt, T. Sangsiri, L. E. Kingsley, and M. Weiner, Appl. Phys. Lett. **62**, 2003 (1993).
[11] D. Some and A. V. Nurmikko, Phys. Rev. B **50**, 5783 (1994).
[12] D. Some and A. V. Nurmikko, Phys. Rev. B **53**, R13 295 (1996).
[13] N. Sarukura, H. Ohtake, S. Izumida, and Z. Liu, J. Appl. Phys. **84**, 654 (1998).
[14] J. N. Heyman, P. Neocleous, D. Herbert, P. A. Cromwell, T. Muller, and K. Unterrainer, Phys. Rev. B **64**, 085202 (2001).
[15] P. Uhd Jepsen, R. H. Jacobsen, and S. R. Keiding, J. Opt. Soc. Am. B **13**, 2424 (1996).
[16] A. Corchia, R. McLaughlin, M. B. Johnston, D. M. Whittaker, D. D. Arnone, E. H. Linfield, A. G. Davies, and M. Pepper, Phys. Rev. B **64**, 205204 (2001).
[17] W. Sha, A. L. Smirl, and W. F. Tseng, Phys. Rev. Lett. **74**, 4273 (1995).
[18] T. Dekorsy, T. Pfeifer, W. Kütt, and H. Kurz, Phys. Rev. B **47**, 3842 (1993).
[19] S. Adachi, J. Appl. Phys. **72**, 3702 (1992).
[20] W. Lukosz, J. Opt. Soc. Am. **69**, 1495 (1979).
[21] J. Shan, C. Weiss, R. Wallenstein, R. Beigang, and T. F. Heinz, Opt. Lett. **26**, 849 (2001).
[22] K. Victor, H. G. Roskos, and C. Waschke, J. Opt. Soc. Am. B **11**, 2470 (1994).
[23] D.-S. Kim and P. Yu, Phys. Rev. B **43**, 4158 (1991).